Title
Orthogonally oriented scaffolds with aligned fibers for engineering intestinal smooth muscle

Authors
Kobayashi, Masae
Lei, Nan Ye
Wang, Qianqian
et al.

Publication Date
2015-08-01

DOI
10.1016/j.biomaterials.2015.05.023

Peer reviewed

HHS Public Access

Author manuscript

Biomaterials. Author manuscript; available in PMC 2016 August 01.

Published in final edited form as:

Biomaterials. 2015 August ; 61: 75–84. doi:10.1016/j.biomaterials.2015.05.023.

Orthogonally oriented scaffolds with aligned fibers for engineering intestinal smooth muscle

Masae Kobayashi[1], **Nan Ye Lei**[1,3], **Qianqian Wang**[1], **Benjamin M. Wu**[1,2], and **James C.Y. Dunn**[1,3,*]

[1]Department of Bioengineering, Henry Samueli School of Engineering, University of California, Los Angeles, Los Angeles, CA 90095, USA

[2]Division of Advanced Prosthodontics & Weintraub Center for Reconstructive Biotechnology, University of California, Los Angeles, CA, USA

[3]Department of Surgery, David Geffen School of Medicine at UCLA, University of California Los Angeles, Los Angeles, CA 90095, USA

Abstract

Controlling cellular alignment is critical in engineering intestines with desired structure and function. Although previous studies have examined the directional alignment of cells on the surface (x-y plane) of parallel fibers, quantitative analysis of the cellular alignment inside implanted scaffolds with oriented fibers has not been reported. This study examined the cellular alignment in the x-z and y-z planes of scaffolds made with two layers of orthogonally oriented fibers. The cellular orientation inside implanted scaffolds was evaluated with immunofluorescence. Quantitative analysis of coherency between cell orientation and fiber direction confirmed that cells aligned along the fibers not only on the surface (x-y plane) but also inside the scaffolds (x-z & y-z planes). Our study demonstrated that two layers of orthogonally aligned scaffolds can generate the histological organization of cells similar to that of intestinal circular and longitudinal smooth muscle.

Keywords

Tissue engineering; cellular alignment; smooth muscle cell; electrospinning; polycaprolactone; scaffold

*Correspondence should be addressed to James Dunn (jdunn@mednet.ucla.edu), MC 709818, CHS 72-140, 10833 Le Conte Avenue, Los Angeles, CA 90095, (310) 206-2429.

Introduction

In the small intestine, the inner circular smooth muscle layer is orthogonally oriented to the outer longitudinal smooth muscle layer, and the myenteric plexus is embedded between these layers. The arrangement of smooth muscle cells, neural cells and interstitial cells of Cajal within the intestinal smooth muscle is highly organized in order to coordinate peristalsis [1]. In other tissues such as the vasculature [2,3], myocardium [4], skeletal muscle [5], nervous system [6,7], and connective tissues [8,9], cellular alignment is also essential for their proper function. It is therefore desirable to replicate the native microstructures and cellular alignment for tissue engineering constructs.

Electrospun scaffolds with aligned fibers have been explored for their suitability to align cells in many tissue engineering applications [5,10–13]. Various synthetic and biological polymers have been electrospun to fabricate scaffolds with desired fiber size and alignment [14,15]. These fibers replicate the length scale of elements in the native extracellular matrix and promote cellular differentiation and matrix production [16,17]. Aligned fibers can be fabricated by collecting elecrospun fibers on rotating mandrels, leading to controllable mechanical and structural anisotropy [5,12,18,19]. Among a variety of FDA approved polymers, poly(3-caprolactone) (PCL) is a promising material due to its biocompatibility, biodegradability and mechanical properties. Fibrous scaffolds composed of PCL are 10 times less stiff and stay elastic over a wider range, as compared to scaffolds made of poly(D,L-lactic- co-glycolic acid 50:50) [20]. Electrospun PCL (ePCL) scaffolds with aligned fibers were shown to enhance cellular alignment, matrix deposition, and increased tensile properties along the fiber direction when compared to similar scaffolds with randomly oriented fibers [5,21]. Such flexibility and controllable directionality of ePCL scaffolds make it a suitable choice for muscle tissue engineering.

Previous studies have examined the cellular alignment on the 2D surface (x-y plane) of cells in culture [2,5–9,22], but the alignment of cells inside 3D scaffolds *in vivo* has not been analyzed quantitatively. We hypothesized that a two-layer ePCL scaffold with orthogonally aligned fibers would generate 3D cellular alignment analogous to the intestinal circular and longitudinal muscle layers. In this study, we compared the cellular alignment in the x-z and y-z planes of implanted ePCL scaffolds made with either aligned or randomly oriented fibers.

Materials and Methods

Electrospinning

11% (w/w) solution of PCL (Durect Lactel, Birmingham, AL) was made in hexafluoro-2-propanol (Acros Organics, Thermo Fisher Scientific, Waltham, MA). The solution was kept on a shaker overnight to obtain a homogenous polymer solution. The mandrel was wrapped with aluminum foil to ease the removal of the scaffold. The PCL solution was transferred to a plastic syringe fitted with an 18-gauge needle, and secured onto a syringe pump (Harvard Apparatus, Holliston, MA). The solution was infused at 2.5 mL/h onto a rotating mandrel collector with an outer diameter of 32 mm that was positioned 12-15 cm away from the needle tip. The electrical potential difference between the needle (i.e., polymer solution) and

the grounded mandrel collector was produced by a high voltage power supply (Glassman High Voltage, High Bridge, NJ). Scaffolds comprised of aligned ePCL fibers were fabricated using a mandrel rotational speed of 3450 rpm and an applied voltage of 15 kV. Less-aligned, “random” ePCL fibers were produced using a mandrel rotational speed of 1725 rpm and applied voltage of 25 kV. After 0.5 mL of polymer solution had been dispensed from the syringe onto the rotating mandrel, the ePCL was carefully removed from the aluminum foil. Scaffolds were air-dried before laser cutting (Fig. 1A).

Scanning Electron Microscopy (SEM)

The surface morphology of ePCL scaffolds with aligned or random fibers was assessed using a Nova NanoSEM 230 (FEI, Hillsboro, Oregon). The scaffolds without conductive coating were mounted on the sticky conductive carbon tape (Ted Pella, Redding, California) on the top of aluminum stubs (Ted Pella, Redding, California) and examined under SEM with an accelerating voltage of 10 kV at low vacuum mode.

Laser cutting

The ePCL scaffolds were constructed as fiber sheets with dimensions approximately 10 × 2.5 cm and thickness of 100-150 μm, based on the mandrel used. These fiber sheets were cut into rectangular 8 × 6.5 mm scaffolds using the VERSA LASER CUTTER 2.3 (Universal Laser Systems, Scottsdale, AZ) with vector mode, 5% power, 100× speed, and 1000 pulses/inch. Two types of scaffolds were obtained by setting the longer or shorter edge of the rectangle to be along the fiber direction (Fig. 1B). The scaffolds were sterilized in 70% ethanol for 30 min and washed several times with phosphate buffered saline (PBS).

Ethics statement

Animal usage complied with regulations set by the University of California, Los Angeles, Chancellor's Animal Research Committee and was approved as animal protocol number 2005-169. All efforts were made to minimize pain and suffering. Two mice strains were used for these experiments: C57BL/6-Tg(Actb-EGFP)1Osb/J (“GFP”) (The Jackson Laboratory, Bar Harbor, ME) and wild type C57BL/6 (Charles River, Wilmington, MA).

Intestinal smooth muscle strips (SMS) isolation and culture

SMS were isolated from two 7 to 8-day-old GFP-positive C57BL/6 neonates using previously described methods [23–25]. The intestines were removed via a midline incision, and smooth muscle strips, containing both longitudinal and circular muscle layers, were gently teased from the intestines using fine forceps and placed in Hank's Balanced Salt Solution without calcium and magnesium (Invitrogen, Carlsbad, CA) on ice. SMS were minced thoroughly using a scalpel. Approximately one-tenth of the SMS were seeded directly to each ePCL scaffold, which was coated with gelatin solution (attachment factor solution; Invitrogen, Carlsbad, CA) at 37°C for at least 30 min and briefly washed with PBS once in advance. SMS-seeded ePCL scaffolds were cultured at 37°C in a 5%CO_2 incubator in Knockout™ D-MEM supplemented with 15% FBS, 0.1 mM 2-mercaptoethanol, 0.1mM non-essential amino acids (NEAA), 2mM L-glutamine, and 1× antibiotic-antimycotic (all from Invitrogen, Carlsbad, CA). The medium was changed after 2 days to the same medium

but without antibiotic-antimycotic. SMS-seeded ePCL scaffolds were incubated *in vitro* for approximately 3 weeks before implantation to allow infiltration of cells inside the scaffolds. The SMS-seeded sides of two ePCL scaffolds were connected together to form a two-layer scaffold with 10 μL of collagen gel (*PureCol*® EZ Gel, Advanced BioMatrix, San Diego, CA) right before implantation (Fig. 1E-H).

Scaffold Implantation

ePCL scaffolds with or without cells were implanted subcutaneously into syngeneic wild type adult C57BL/6 mice. Recipient mice were anesthetized with inhaled isoflurane and given a subcutaneous injection of 0.05 mg/kg buprenorphine. The abdomen was shaved, prepared, and draped sterilely. A ventral midline incision was made and skin flaps were raised laterally to create subcutaneous pockets. The ePCL scaffolds were sutured to the abdominal wall using 6-0 Prolene suture (Ethicon, Somerville, NJ), and the incision was closed using 3-0 silk suture (Ethicon). Recipient mice with SMS-seeded scaffolds were sacrificed approximately 4 days postoperatively while recipient mice with scaffolds without initial SMS seeding were sacrificed approximately 2 weeks postoperatively. The explants were formalin-fixed and processed for histological evaluations.

Histology & immunofluorescence staining

In vivo explants were fixed and processed for paraffin embedding. Serial 5-μm sections were cut and adhered to glass slides; every third slide was stained with hematoxylin and eosin (HE). Unstained slides were prepared for immunofluorescence staining. Slides were de-waxed with xylene and rehydrated with serial dilutions of ethanol. Next, slides were incubated in a citric buffer (Biogenex, San Ramon, CA) for 15 min at 95-100°C and allowed to cool for 15 minutes in an over flowing water bath. *In vitro* cultures were fixed without histologic processing. After three washes with PBS, samples were treated with blocking buffer containing 5% normal goat serum (Vector Labs, Burlingame, CA), 0.1% Triton X-100 (Sigma) in PBS for 1 hour at 4°C. Samples were then incubated with primary antibodies against alpha smooth muscle actin (α-SMA) (1:250; Dako, Carpinteria, CA) and green fluorescent protein (GFP) (1:1000, Abcam, Cambridge, MA) diluted in blocking buffer overnight at 4°C. After two washes in PBS, samples were incubated in the dark with their corresponding secondary antibodies (goat anti-mouse Alexa Fluor 488, goat anti-rabbit Alexa Fluor 596, Invitrogen) diluted at 1:1000 in blocking buffer for 2 hours at room temperature. After three washes with PBS, Prolong Gold with DAPI (Invitrogen) was applied to each section and the slides were covered with glass coverslips. Then, slides were allowed to cure at 4°C before storing at −80°C. Images were acquired with an Olympus IX71 microscope with cellSens software (Olympus, Center Valley, PA).

Quantification of cellular alignment inside ePCL

Immunofluorescence of α-SMA and GFP was used to assess the alignment of cells within the ePCL scaffold. The alignment measurement was carried out with the NIH ImageJ software plug-in named OrientationJ to calculate the directional coherency coefficient [26]. The coherency coefficient ranges from 0 to 1, with 1 indicating a strongly coherent orientation or for this study, greater cellular alignment. To assess the fiber orientation of

bare ePCL scaffolds, 3 sample areas were captured. To assess the cell orientation on the surface of the ePCL scaffold under *in vitro* culture, 3 sample areas were captured for both α-SMA and GFP immunostaining. The alignment of cells inside the ePCL scaffold was evaluated at the following four experimental configurations: (1) aligned ePCL scaffold without SMS seeding, 2 weeks *in vivo*. Approximately 100 sample areas of 6 scaffolds from 4 different animals were analyzed. (2) random ePCL scaffold without SMS seeding, 2 weeks *in vivo*. Approximately 140 sample areas of 4 scaffolds from 2 different animals were analyzed. (3) aligned ePCL scaffold with SMS seeding, 3 weeks *in vitro* culture followed by 4 days *in vivo*. Approximately 200 sample areas of 6 scaffolds from 3 different animals were analyzed for α-SMA expression and 43 sample areas of 3 scaffolds from 3 different animals were analyzed for GFP expression. (4) random ePCL with SMS seeding, 3 weeks *in vitro* culture followed by 4 days *in vivo*. Approximately 140 sample areas of 4 scaffolds from 2 different animals were analyzed for α-SMA expression and 55 sample areas of 3 scaffolds from 2 different animals were analyzed for GFP expression. For each condition, sample areas were grouped into the upper or lower layer of the x-z or y-z plane and their coherency were compared (Fig. 1E-H).

Statistical Analysis

Two-tailed unpaired Student's t-test was used to compare the results from the image analysis. A level of significance was set at $p < 0.01$. Data were expressed as the mean ± the standard deviation (SD).

Results

Two-layer Scaffolds

The intestinal circular and longitudinal smooth muscle layers are orthogonally arranged relative to each other (Fig. 1C,D). To mimic this native histological organization, we employed two layers of ePCL scaffolds with aligned fibers seeded with or without SMS. Scaffolds with randomly oriented fibers seeded with or without SMS were used as comparisons. Two layers of the ePCL scaffolds were assembled from either aligned or randomly oriented fibers by adding collagen gel between two sheets of ePCL. In order to examine the cellular alignment inside the ePCL scaffolds, two-layer scaffolds were cut in orthogonal planes to expose cross sections in x-z and y-z planes (Fig. 1). For the two-layer scaffold with aligned fibers arranged in orthogonal directions, the cross section exposing the x-z plane would cut “perpendicular” to aligned fibers in the upper layer (shown in blue in Fig. 1F) and “parallel” to aligned fibers in the lower layer (shown in green in Fig. 1F). Conversely, the cross section exposing the y-z plane would cut “parallel” to aligned fibers in the upper layer (shown in blue in Fig. 1F) and “perpendicular” to aligned fibers in the lower layer (shown in green in Fig. 1F). In contrast, the ePCL construct with two layers of randomly oriented fibers would appear similar in the x-z and y-z plane cross sections (Fig. 1H).

Scaffold characterization

The difference between ePCL scaffolds with aligned or randomly oriented fibers was examined by SEM (Fig. 2A-D). Aligned ePCL scaffolds had individual fibers 1-5 μm in

diameter and most fibers existed individually without crossover (Fig. 2C). Randomly oriented ePCL scaffolds had similar fiber size, with most fibers intertwined with each other (Fig. 2D). Analysis of the fibers showed that the coherency factor of aligned ePCL scaffolds was statistically higher (0.555±0.058 vs. 0.060±0.030; $p = 1.91e-04 < 0.01$) than that of the randomly oriented ePCL scaffolds (Fig. 2E).

Quantification of in vitro cellular alignment (x-y plane)

Following two weeks of culture *in vitro*, the difference in alignment of cells on the surface of aligned and randomly oriented ePCL scaffolds (x-y plane) was evaluated by the expression of α-SMA (Fig. 2G,H) and GFP (Fig. 2J,K). Analysis of the coherency factor from immunostained images showed that cells cultured on aligned ePCL scaffolds were statistically more aligned (α-SMA: 0.385±0.023 vs. 0.103±0.011; $p = 4.36e-05 < 0.01$, GFP: 0.309±0.013 vs. 0.079±0.013; $p = 2.75e-05 < 0.01$) than cells cultured on randomly oriented ePCL scaffolds for both markers (Fig. 2F,I).

Quantification of infiltrating host cells' alignment inside two-layer ePCL scaffolds (x-z and y-z planes)

After two weeks of implantation, the alignment of infiltrating host cells into the two-layer ePCL scaffolds without seeded SMS was analyzed by immnuostaining for α-SMA and by HE (Fig. 3,4). Host cell infiltration inside ePCL scaffolds with two layers of orthogonally aligned fibers (Fig. 3) mimicked the cellular alignment of intestinal circular and longitudinal smooth muscle layers (Fig. 1C,D). The alignment of upper and lower layers was completely exchanged when the cross section was switched from the x-z to the y-z plane. The upper layer had “perpendicular” and lower layer had “parallel” alignment to the cross sections in x-z plane, while the upper layer had “parallel” and lower layer had “perpendicular” alignment to the cross sections in y-z plane (Fig. 3A-D). In contrast, the upper and lower layers in ePCL scaffolds with randomly oriented fibers demonstrated similar cellular alignment for both cross sections in the x-z and y-z planes (Fig. 4A-D).

Coherency analysis of α-SMA expression for two-layer ePCL scaffolds with aligned fibers confirmed that cells in the lower layer were statistically more aligned (0.402±0.039 vs. 0.191±0.045; $p = 2.22e-05 < 0.01$) than cells in the upper layer in x-z plane, while cells in the upper layer were statistically more aligned (0.424±0.039 vs. 0.212±0.055; $p = 1.59e-05 < 0.01$) than cells in the lower layer in y-z plane (Fig. 3E). The coherency distribution in the x-z plane showed that most of the cells in lower layer were more aligned than those in the upper layer with little overlap (Fig. 3F).

In contrast, coherency analysis of α-SMA expression for two-layer ePCL scaffolds with randomly oriented fibers demonstrated no statistical difference in cellular alignment between upper and lower layers in both x-z plane cross sections (0.334±0.056 vs. 0.345±0.055; $p = 0.798 > 0.01$) and y-z plane cross sections (0.355±0.014 vs. 0.313±0.023; $p = 0.020 > 0.01$) (Fig. 4E). The coher ency distribution in the x-z plane showed that most of the cells in upper and lower layers had similar cellular alignment, as demonstrated by the extensive overlap (Fig. 4F).

Quantification of cellular alignment inside SMS-seeded two-layer ePCL scaffolds (x-z and y-z planes)

After three weeks of *in vitro* culture followed by 4 days of implantation, cellular alignment inside SMS-seeded two-layer ePCL scaffolds was analyzed by HE staining and immunostaining for α-SMA (Fig. 5,6) and GFP (Fig. 7,8). Since α-SMA and HE stained cells from both seeded SMS and host, GFP was used to examine the cellular alignment from seeded SMS.

Similar to the infiltrating host cells, the alignment of GFP-positive cells in upper and lower layers in aligned ePCL scaffolds was completely reversed when the cross section was switched from the x-z to the y-z plane. The upper layer had “perpendicular” and lower layer had “parallel” alignment to the cross sections in x-z plane, while the upper layer had “parallel” and lower layer had “perpendicular” alignment to the cross sections in y-z plane (Fig. 5A-D, 7A-D). Conversely, GFP-positive cells in the upper and lower layers in ePCL scaffolds with randomly oriented fibers demonstrated similar cellular alignment for both cross sections in the x-z and y-z planes (Fig. 6A-D, 8A-D). Coherency analysis of α-SMA and GFP expressions for aligned two-layer ePCL scaffolds again demonstrated that cells in the lower layer were statistically more aligned (α-SMA: 0.416±0.032 vs. 0.238±0.040; $p = 6.85e\text{-}06 < 0.01$, GFP: 0.423±0.017 vs. 0.251±0.041; $p = 2.47e\text{-}03 < 0.01$) than cells in the upper layer in x-z plane, while cells in the upper layer were statistically more aligned (α-SMA: 0.458±0.050 vs. 0.178±0.029; $p = 6.85e\text{-}06 < 0.01$, GFP: 0.517±0.047 vs. 0.277±0.028; $p = 1.60e\text{-}03 < 0.01$) than cells in the lower layer in y-z plane (Fig. 5E, 7E). The coherency distribution in x-z plane showed that most of the cells in lower layer were more aligned than those in the upper layer with little overlap (Fig. 5F, 7F).

In contrast, coherency analysis of α-SMA and GFP expressions for random two-layer ePCL scaffolds showed no statistical differences in cellular alignment between upper and lower layers in both x-z plane cross sections (α-SMA: 0.351±0.059 vs. 0.347±0.020; $p = 0.909 > 0.01$, GFP: 0.373±0.033 vs. 0.389±0.008; $p = 0.461 > 0.01$) and y-z plane cross sections (α-SMA: 0.309±0.041 vs. 0.327±0.043; $p = 0.565 > 0.01$, GFP: 0.357±0.038 vs. 0.373±0.046; $p = 0.664 > 0.01$) (Fig. 6E, 8E). The coherency distribution in x-z plane showed that most of the cells in upper and lower layers had similar cellular alignment with extensive overlap (Fig. 6F, 8F).

Summary of cellular alignment inside two-layer ePCL scaffolds (x-z and y-z planes)

For both x-z and y-z planes of two-layer ePCL scaffolds with orthogonally aligned fibers, the highest coherency factor was associated with cross sections that were cut “parallel” to aligned fibers (above 0.4), whereas the coherency factor was significantly lower when cross sections were taken “perpendicular” to aligned fibers (below 0.3). The layers of randomly aligned ePCL scaffolds consistently had average coherency factors that fell between 0.3 and 0.4 (Fig. 3-8E). In addition, the coherency distribution of x-z plane analysis displayed Gaussian distribution (Fig. 3-8F). These results occurred for cells from both host and seeded SMS, thus validating that the fiber alignment of ePCL had influenced the cellular alignment inside two-layer scaffolds (Fig. 3-8).

Discussion

We demonstrated that orthogonally aligned ePCL scaffolds could induce cellular alignment similar to intestinal circular and longitudinal smooth muscle layers. In contrast, ePCL scaffolds with randomly oriented fibers did not produce such distinguishable cellular alignment. Cells from both seeded SMS and host infiltrated into the entire depth of the two-layer ePCL scaffolds. These results suggested that cells tended to elongate along the fiber direction not only on the surface of ePCL, but also inside the ePCL after infiltration.

While previous studies have shown 2D cellular alignment with oriented fibers (x-y plane) [2,5–9,22], our study has demonstrated that this approach is also applicable to 3D cellular alignment in vivo (x-z and y-z planes). We chose FDA-approved ePCL as scaffolds for clinically translatable practice. As a result, with only gelatin coating of the ePCL, cells from both seeded SMS and host aligned and elongated along the fiber directions inside the ePCL scaffolds. This system can be useful in tissue regeneration where alignment is essential: vasculature [2,3,27], myocardial tissue [4], musculoskeletal tissue [5], nervous system [6,7], and connective tissue [8,9].

A prior study suggested that the loss of architecture due to rapid degradation of the scaffold prior to the completion of tissue remodeling could impair cellular alignment and cause scar formation [28]. However, ePCL *in vivo* degradation studies showed only 20-30% molecular weight reduction after 3-6 months, without structural deterioration [28–31]. Similarly, in our study, there was no significant degradation of the scaffold at explantation, and ePCL fibers could still been seen on histology. Whether the observed cellular alignment will persist after ePCL degradation is unclear. The cells may still maintain their orientation because the extracellular matrix that replaced the ePCL fibers may also be aligned [32]. Future studies are needed to evaluate the longevity of cellular alignment after degradation of the ePCL.

Our ultimate goal is to construct fully functional intestinal smooth muscle layers capable of peristalsis. Future studies will use this system as a foundation to mimic the intestinal smooth muscle layers, by adding additional components into the two orthogonally aligned ePCL scaffolds. For example, purified enteric neuronal cells and interstitial cells of Cajal can be seeded in-between the two-layer ePCL scaffolds to serve as the myenteric plexus and aid intestinal smooth muscle cells by providing the necessary signals for peristalsis. Intestinal constructs fabricated from this two-layer aligned ePCL may be used to generate full-thickness intestine useful for the treatment of short bowel syndrome or inflammatory bowel disease [33–36].

Conclusions

Our study demonstrated that orthogonally aligned ePCL scaffolds can regenerate the cellular alignment of native intestinal circular and longitudinal smooth muscle layers. Our analysis quantitatively confirmed that cells align along the ePCL fibers not only on the surface (x-y plane) but also inside of the ePCL scaffolds (x-z & y-z planes). Future development of this system by adding myenteric plexus components will promote the creation of more functional intestinal smooth muscle layers. Similarly, this system can be applied to other

types of tissues engineering that require alignment. Our investigation validated the significance of fiber alignment within scaffolds for engineering three dimensionally aligned tissues.

Acknowledgments

We thank UCLA Translational Pathology Core Lab for histologic processing. This work was funded by an R01 DK083119 from the National Institutes of Health.

References

1. Bitar KN, Raghavan S, Zakhem E. Tissue engineering in the gut: developments in neuromusculature. Gastroenterology. 2014; 146:1614–24.10.1053/j.gastro.2014.03.044 [PubMed: 24681129]
2. Chiu JJ, Chen LJ, Chen CN, Lee PL, Lee CI. A model for studying the effect of shear stress on interactions between vascular endothelial cells and smooth muscle cells. J Biomech. 2004; 37:531–9.10.1016/j.jbiomech.2003.08.012 [PubMed: 14996565]
3. Nerem RM, Seliktar D. Vascular tissue engineering. Annu Rev Biomed Eng. 2001; 3:225–43.10.1146/annurev.bioeng.3.1.225 [PubMed: 11447063]
4. Papadaki M, Bursac N, Langer R, Merok J, Vunjak-Novakovic G, Freed LE. Tissue engineering of functional cardiac muscle: molecular, structural, and electrophysiological studies. Am J Physiol Hear Circ Physiol. 2001; 280:H168–78.
5. Li WJ, Mauck RL, Cooper Ja, Yuan X, Tuan RS. Engineering controllable anisotropy in electrospun biodegradable nanofibrous scaffolds for musculoskeletal tissue engineering. J Biomech. 2007; 40:1686–93.10.1016/j.jbiomech.2006.09.004 [PubMed: 17056048]
6. Yang F, Murugan R, Wang S, Ramakrishna S. Electrospinning of nano/micro scale poly(L-lactic acid) aligned fibers and their potential in neural tissue engineering. Biomaterials. 2005; 26:2603–10.10.1016/j.biomaterials.2004.06.051 [PubMed: 15585263]
7. Kim YT, Haftel VK, Kumar S, Bellamkonda RV. The role of aligned polymer fiber-based constructs in the bridging of long peripheral nerve gaps. Biomaterials. 2008; 29:3117–27.10.1016/j.biomaterials.2008.03.042 [PubMed: 18448163]
8. Liu Y, Ramanath HS, Wang DA. Tendon tissue engineering using scaffold enhancing strategies. Trends Biotechnol. 2008; 26:201–9.10.1016/j.tibtech.2008.01.003 [PubMed: 18295915]
9. Vunjak-Novakovic G, Altman G, Horan R, Kaplan DL. Tissue engineering of ligaments. Annu Rev Biomed Eng. 2004; 6:131–56.10.1146/annurev.bioeng.6.040803.140037 [PubMed: 15255765]
10. Ionescu LC, Mauck RL. Porosity and Cell Preseeding Influence Electrospun Scaffold Maturation and Meniscus Integration In Vitro. Tissue Eng Part A. 2013; 19:538–47.10.1089/ten.tea.2012.0052 [PubMed: 22994398]
11. Ayres C, Bowlin GL, Henderson SC, Taylor L, Shultz J, Alexander J, et al. Modulation of anisotropy in electrospun tissue-engineering scaffolds: Analysis of fiber alignment by the fast Fourier transform. Biomaterials. 2006; 27:5524–34.10.1016/j.biomaterials.2006.06.014 [PubMed: 16859744]
12. Courtney T, Sacks MS, Stankus J, Guan J, Wagner WR. Design and analysis of tissue engineering scaffolds that mimic soft tissue mechanical anisotropy. Biomaterials. 2006; 27:3631–8.10.1016/j.biomaterials.2006.02.024 [PubMed: 16545867]
13. Reneker DH, Chun I. Nanometre diameter fibres of polymer, produced by electrospinning. Nanotechnology. 1996; 7:216–23.10.1088/0957-4484/7/3/009
14. Li M, Mondrinos MJ, Gandhi MR, Ko FK, Weiss AS, Lelkes PI. Electrospun protein fibers as matrices for tissue engineering. Biomaterials. 2005; 26:5999–6008.10.1016/j.biomaterials.2005.03.030 [PubMed: 15894371]
15. Xu C, Yang F, Wang S, Ramakrishna S. In vitro study of human vascular endothelial cell function on materials with various surface roughness. J Biomed Mater Res A. 2004; 71:154–61.10.1002/jbm.a.30143 [PubMed: 15368265]

16. Li WJ, Jiang YJ, Tuan RS. Chondrocyte phenotype in engineered fibrous matrix is regulated by fiber size. Tissue Eng. 2006; 12:1775–85.10.1089/ten.2006.12.1775 [PubMed: 16889508]
17. Lee CH, Shin HJ, Cho IH, Kang YM, Kim IA, Park KD, et al. Nanofiber alignment and direction of mechanical strain affect the ECM production of human ACL fibroblast. Biomaterials. 2005; 26:1261–70.10.1016/j.biomaterials.2004.04.037 [PubMed: 15475056]
18. Nerurkar NL, Elliott DM, Mauck RL. Mechanics of Oriented Electrospun Nanofibrous Scaffolds for Annulus Fibrosus Tissue Engineering. 2007:1018–28.10.1002/jor
19. Ayres CE, Bowlin GL, Pizinger R, Taylor LT, Keen Ca, Simpson DG. Incremental changes in anisotropy induce incremental changes in the material properties of electrospun scaffolds. Acta Biomater. 2007; 3:651–61.10.1016/j.actbio.2007.02.010 [PubMed: 17513181]
20. Li WJ, Cooper Ja, Mauck RL, Tuan RS. Fabrication and characterization of six electrospun poly(alpha-hydroxy ester)-based fibrous scaffolds for tissue engineering applications. Acta Biomater. 2006; 2:377–85.10.1016/j.actbio.2006.02.005 [PubMed: 16765878]
21. Baker BM, Mauck RL. The effect of nanofiber alignment on the maturation of engineered meniscus constructs. Biomaterials. 2007; 28:1967–77.10.1016/j.biomaterials.2007.01.004 [PubMed: 17250888]
22. Baker BM, Gee AO, Metter RB, Nathan AS, Marklein RA, Burdick JA, et al. The potential to improve cell infiltration in composite fiber-aligned electrospun scaffolds by the selective removal of sacrificial fibers. Biomaterials. 2008; 29:2348–58. [PubMed: 18313138]
23. Geisbauer CL, Chapin JC, Wu BM, Dunn JCY. Transplantation of Enteric Cells Expressing p75 in the Rodent Stomach. J Surg Res. 2012; 174:257–65.10.1016/j.jss.2010.12.016 [PubMed: 21324400]
24. Ordög T, Redelman D, Horowitz NN, Sanders KM. Immunomagnetic enrichment of interstitial cells of Cajal. Am J Physiol Gastrointest Liver Physiol. 2004; 286:G351–60.10.1152/ajpgi.00281.2003 [PubMed: 14563669]
25. Walthers CM, Lee M, Wu BM, Dunn JCY. Smooth muscle strips for intestinal tissue engineering. PLoS One. 2014; 9:e114850.10.1371/journal.pone.0114850 [PubMed: 25486279]
26. Fonck E, Feigl GG, Fasel J, Sage D, Unser M, Rüfenacht Da, et al. Effect of aging on elastin functionality in human cerebral arteries. Stroke. 2009; 40:2552–6.10.1161/STROKEAHA.108.528091 [PubMed: 19478233]
27. Xu C. Aligned biodegradable nanofibrous structure: a potential scaffold for blood vessel engineering. Biomaterials. 2004; 25:877–86.10.1016/S0142-9612(03)00593-3 [PubMed: 14609676]
28. Lorden ER, Miller KJ, Bashirov L, Ibrahim MM, Hammett E, Jung Y, et al. Mitigation of hypertrophic scar contraction via an elastomeric biodegradable scaffold. Biomaterials. 2015; 43:61–70.10.1016/j.biomaterials.2014.12.003 [PubMed: 25591962]
29. Bölgen N, Menceloğlu YZ, Acatay K, Vargel i, Pişkin E. In vitro and in vivo degradation of non-woven materials made of poly(ε-caprolactone) nanofibers prepared by electrospinning under different conditions. J Biomater Sci Polym Ed. 2005; 16:1537–55.10.1163/156856205774576655 [PubMed: 16366336]
30. Pektok E, Nottelet B, Tille JC, Gurny R, Kalangos A, Moeller M, et al. Degradation and Healing Characteristics of Small-Diameter Poly(-Caprolactone) Vascular Grafts in the Rat Systemic Arterial Circulation. Circulation. 2008; 118:2563–70.10.1161/CIRCULATIONAHA.108.795732 [PubMed: 19029464]
31. Tillman BW, Yazdani SK, Lee SJ, Geary RL, Atala A, Yoo JJ. The in vivo stability of electrospun polycaprolactone-collagen scaffolds in vascular reconstruction. Biomaterials. 2009; 30:583–8.10.1016/j.biomaterials.2008.10.006 [PubMed: 18990437]
32. Petrigliano FA, Arom GA, Nazemi AN, Yeranosian MG, Wu BM, McAllister DR. In Vivo Evaluation of Electrospun Polycaprolactone Graft for Anterior Cruciate Ligament Engineering. Tissue Eng Part A. 2014 150127064142004. 10.1089/ten.tea.2013.0482
33. Hanauer SB. Inflammatory bowel disease: Epidemiology, pathogenesis, and therapeutic opportunities. Inflamm Bowel Dis. 2006; 12:S3–9.10.1097/01.MIB.0000195385.19268.68 [PubMed: 16378007]

34. Abraham C, Cho JH. Inflammatory bowel disease. N Engl J Med. 2009; 361:2066–78.10.1056/NEJMra0804647 [PubMed: 19923578]

35. Kim ER, Chang DK. Colorectal cancer in inflammatory bowel disease: The risk, pathogenesis, prevention and diagnosis. World J Gastroenterol. 2014; 20:9872–81.10.3748/wjg.v20.i29.9872 [PubMed: 25110418]

36. Coviello LC, Stein SL. Surgical management of nonpolypoid colorectal lesions and strictures in colonic inflammatory bowel disease. Gastrointest Endosc Clin N Am. 2014; 24:447–54.10.1016/j.giec.2014.04.002 [PubMed: 24975535]

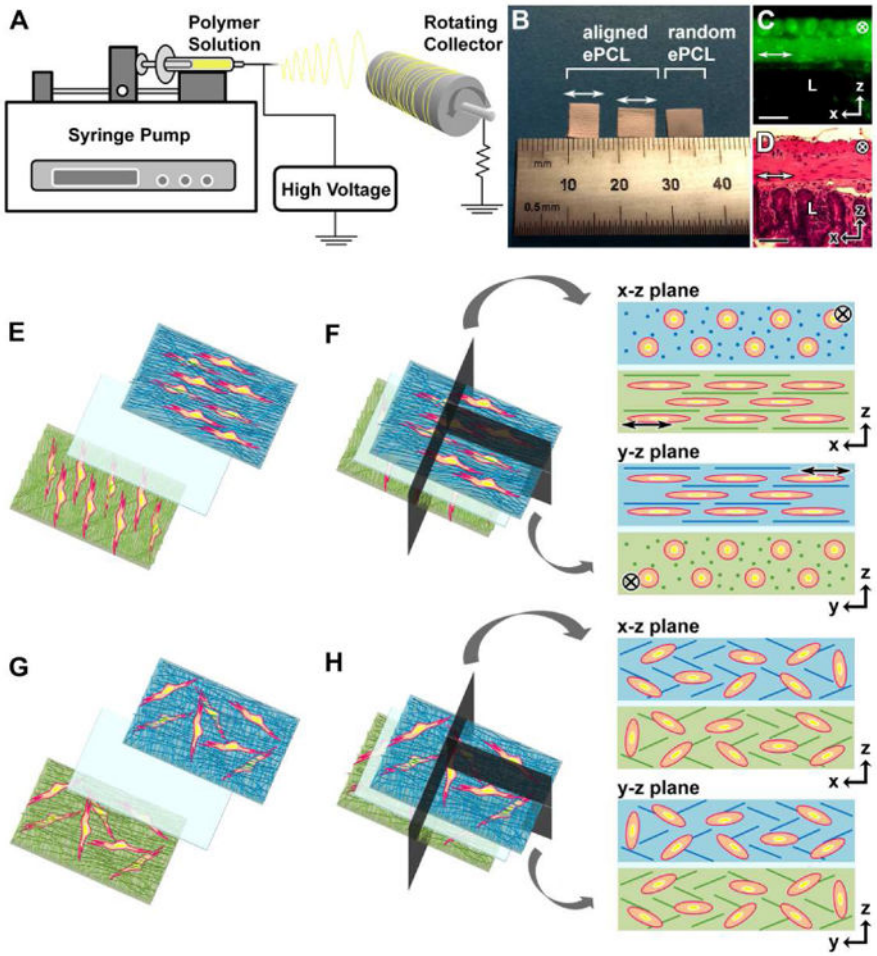

Fig. 1.

Schematic diagram of two-layer scaffolds for mimicking small intestine layers. (A) Basic setup for fabricating electrospun polypolycaprolactone (ePCL) sheets. (B) Laser cut ePCL scaffolds with aligned and random fibers. (C) Immunofluorescence of smooth muscle actin (α-SMA) expression and (D) HE staining of adult, mouse small intestine in cross section. Preparation of two-layer ePCL scaffolds with (E) aligned or (G) randomly oriented fibers for implantation. In order to mimic the intestinal circular and longitudinal muscle layers, two-layer ePCL scaffolds with orthogonally oriented fibers were seeded with intestinal smooth muscles strips (SMS) and connected with a thin collagen gel before implantation. Two-layer ePCL scaffolds with randomly oriented fibers were used as controls. To compare the cell alignment inside the ePCL, two-layer scaffolds with (F) aligned or (H) randomly oriented fibers were cut in two perpendicular planes to expose cross sections in x-z and y-z planes. Scale bar = 50 μm. L = Lumen. ⊗ = alignment perpendicular to the cross section. ↔ = alignment parallel to the cross section.

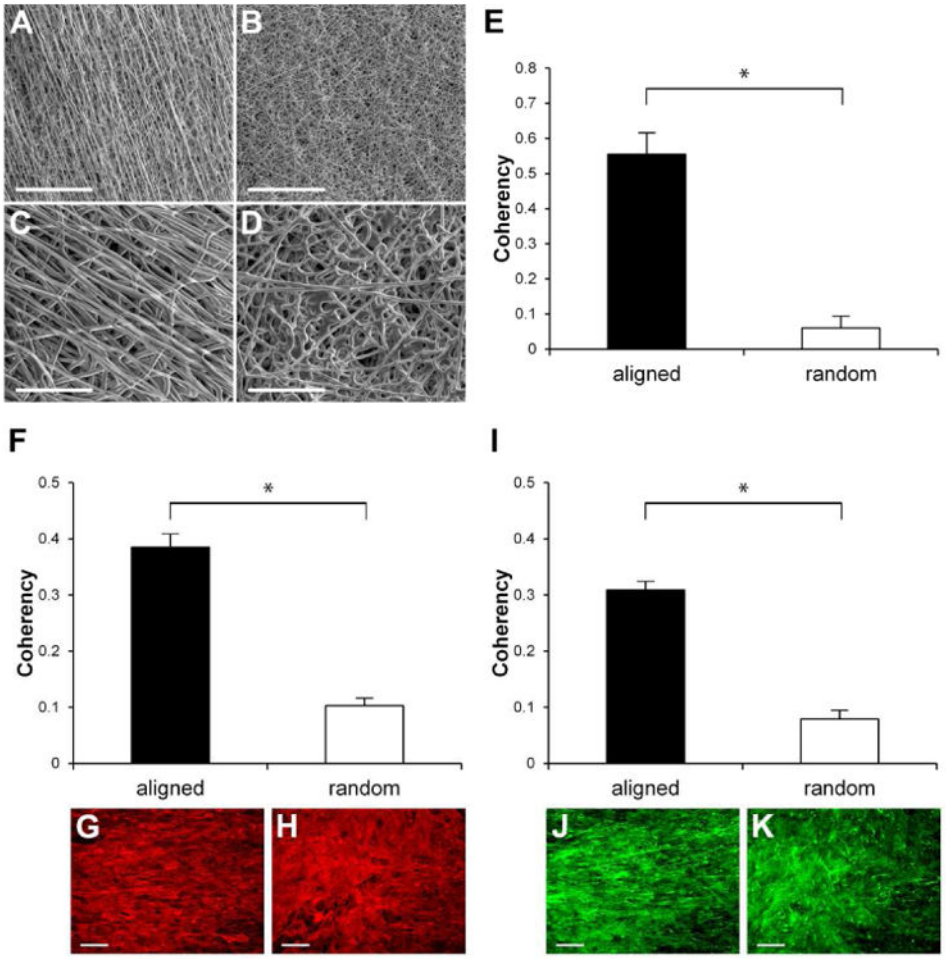

Fig. 2.

Alignment of cells on SMS-seeded ePCL scaffolds. Scanning electron micrographs of ePCL with (A, C) aligned and (B, D) randomly oriented fibers at 250× and 1000× magnifications. (E) Coherency analysis of aligned and random ePCL (n=3). Scaffolds were seeded with SMS and immunostained at day 14. Images were taken to show the cell alignment on the ePCL surface (x-y plane). (G, H) α-SMA and (J, K) green fluorescent protein (GFP) expression of SMS seeded on (G, J) aligned and (H, K) random ePCL. Coherency analysis of (F) α-SMA (n=3) and (I) GFP (n=3) expression of SMS seeded on aligned and random ePCL. *$p < 0.01$. Error bar = SD. Scale bar A, B, G, H, J, K = 200 μm; scale bar C, D = 50 μm.

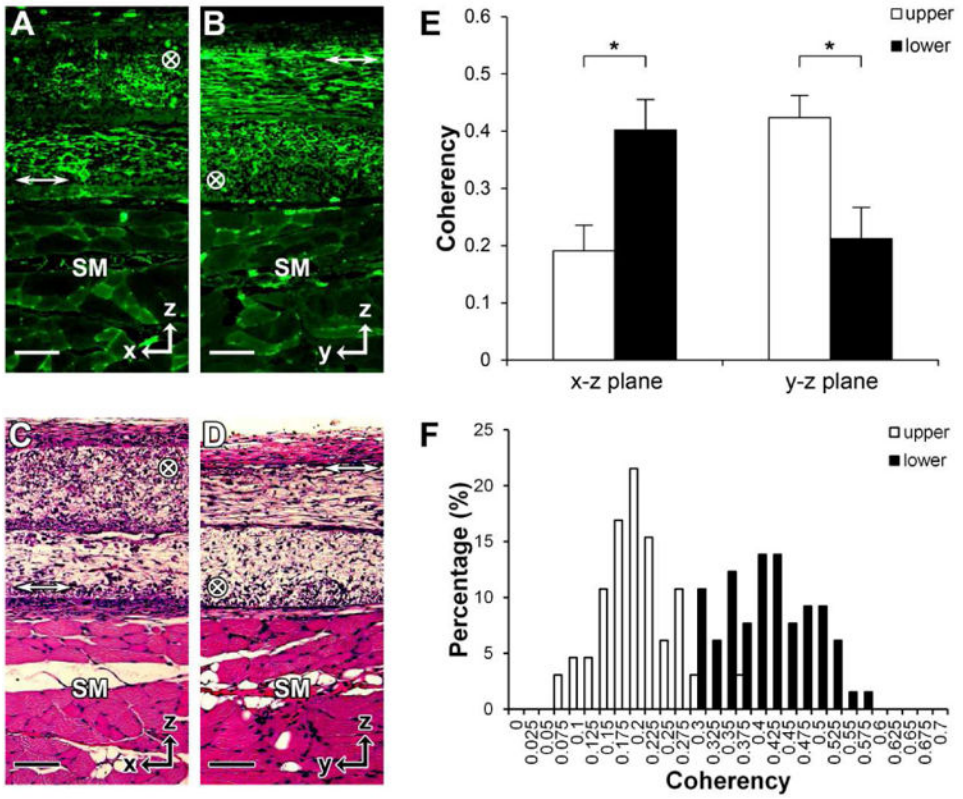

Fig. 3.

Quantification of α-SMA alignment expressed by infiltrating host cells inside two-layer ePCL scaffolds with aligned fibers. ePCL scaffolds were retrieved on day 14 after implantation. α-SMA expression of infiltrating host cells inside aligned ePCL scaffolds in the (A) x-z and (B) y-z planes. HE staining of infiltrating host cells inside aligned ePCL scaffolds on the (C) x-z and (D) y-z planes. (E) Coherency analysis and (F) the distribution (x-z plane as representative) of α-SMA alignment of infiltrating host cells inside two-layer aligned ePCL scaffolds (n=6). *$p < 0.01$. Error bar = SD. Scale bar = 100 μm. SM = Skeletal M uscle. ⊗ = alignment perpendicular to the cross section. ↔ = alignment parallel to the cross section.

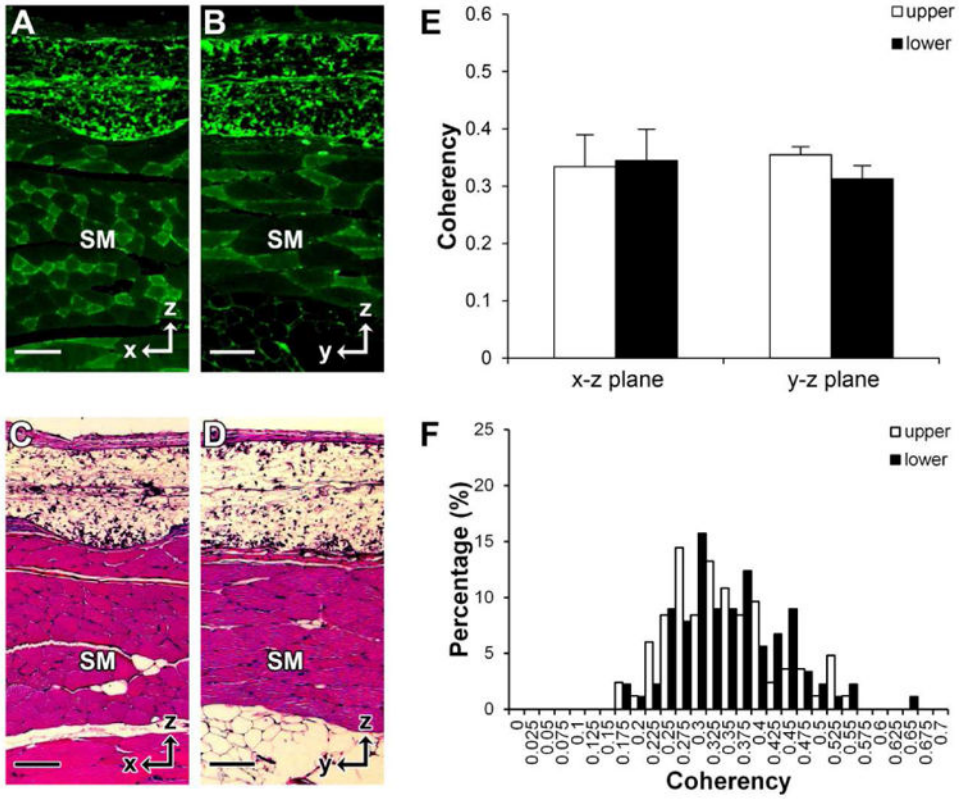

Fig. 4.

Quantification of α-SMA alignment of infiltrating host cells inside two-layer ePCL scaffolds with randomly oriented fibers. ePCL scaffolds were retrieved on day 14 after implantation. α-SMA expression of infiltrating host cells inside randomly oriented ePCL scaffolds on the (A) x-z and (B) y-z planes. HE staining of infiltrating host cells inside randomly oriented ePCL scaffolds on the (C) x-z and (D) y-z planes. (E) Coherency analysis and (F) the distribution (x-z plane as representative) of α-SMA alignment of infiltrating host cells inside two-layer random ePCL scaffolds (n=4). $p > 0.01$. Error bar = SD. Scale bar = 100 μm. SM = Skeletal Muscle.

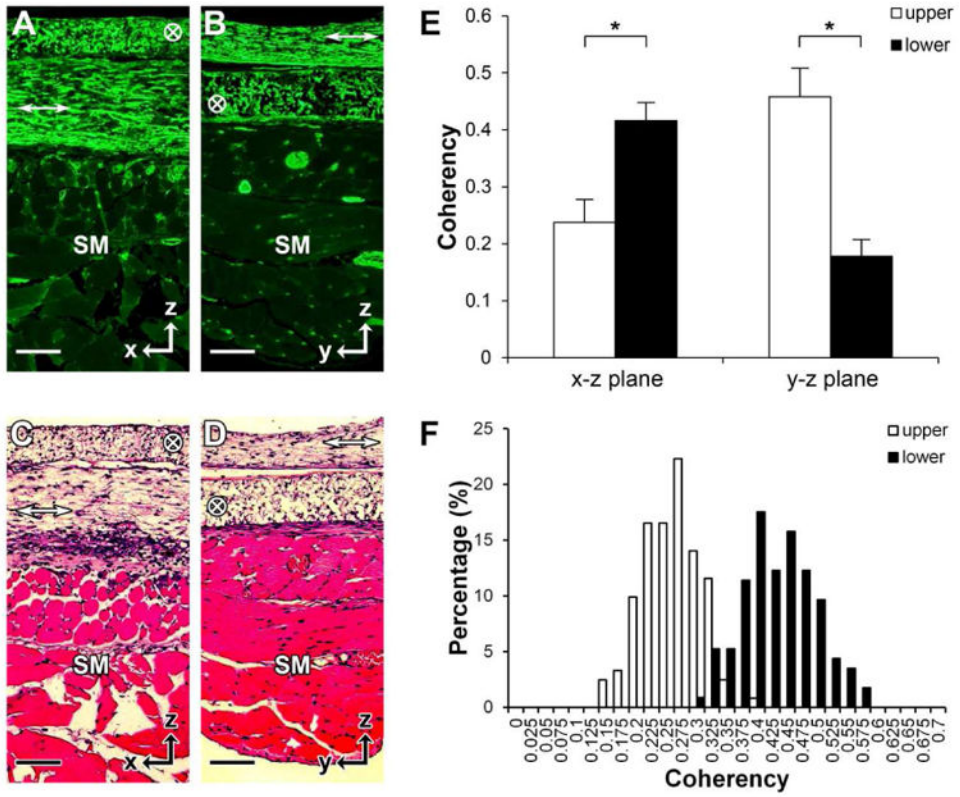

Fig. 5.

Quantification of α-SMA alignment of seeded SMS and infiltrating host cells inside two-layer ePCL scaffolds with aligned fibers. ePCL scaffolds were cultured *in vitro* for 3 weeks and retrieved on day 4 after implantation. α-SMA expression of seeded SMS and infiltrating host cells inside aligned ePCL scaffolds on the (A) x-z and (B) y-z planes. HE staining of seeded SMS and infiltrating host cells inside aligned ePCL scaffolds on the (C) x-z and (D) y-z planes. (E) Coherency analysis and (F) the distribution (x-z plane as representative) of α-SMA alignment of seeded SMS and infiltrating host cells inside two-layer aligned ePCL scaffolds (n=6). *$p < 0.01$. Error bar = SD. Scale bar = 100 μm. SM = Skeletal Muscle. ⊗ = alignment perpendicular to the cross section. ↔ = alignment parallel to the cross section.

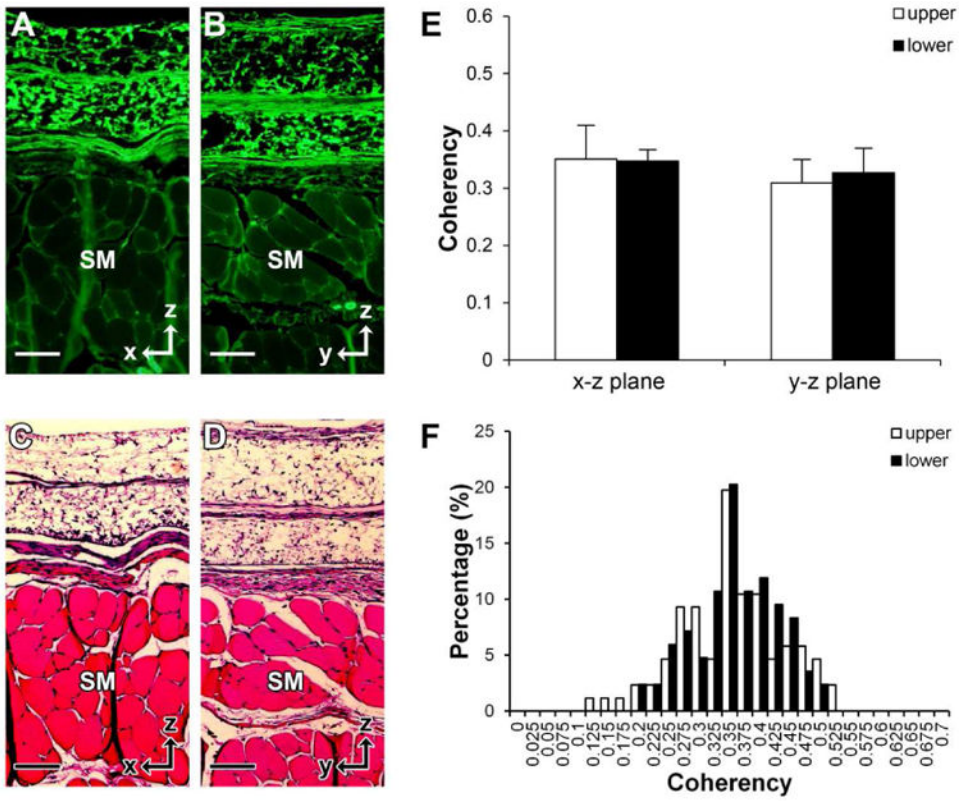

Fig. 6.

Quantification of α-SMA alignment of seeded SMS and infiltrating host cells inside two-layer ePCL scaffolds with randomly oriented fibers. ePCL scaffolds were cultured *in vitro* for 3 weeks and retrieved on day 4 after implantation. α-SMA expression of seeded SMS and infiltrating host cells inside randomly oriented ePCL scaffolds on the (A) x-z and (B) y-z planes. HE staining of seeded SMS and infiltrating host cells inside randomly oriented ePCL scaffolds on the (C) x-z and (D) y-z planes. (E) Coherency analysis and (F) the distribution (x-z plane as representative) of α-SMA alignment of seeded SMS and infiltrating host cells inside two-layer random ePCL scaffolds (n=4). $p > 0.01$. Error bar = SD. Scale bar = 100 μm. SM = Skeletal Muscle.

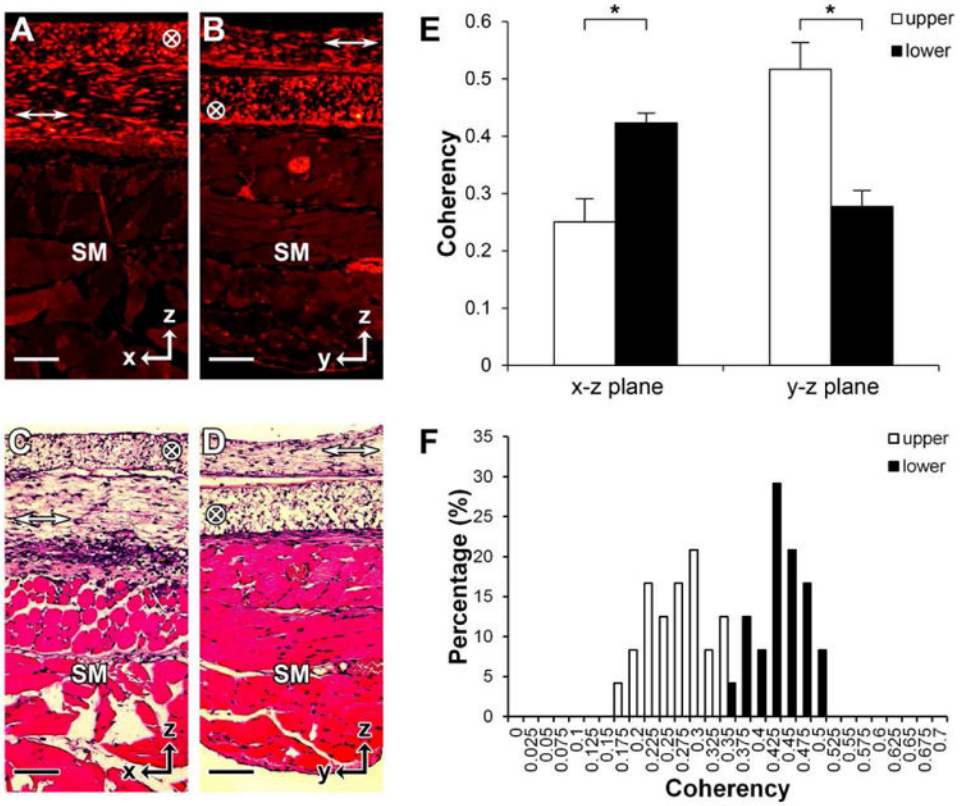

Fig. 7.

Quantification of GFP alignment of seeded SMS inside two-layer ePCL scaffolds with aligned fibers. ePCL scaffolds were cultured *in vitro* for 3 weeks and retrieved on day 4 after implantation. GFP expression of seeded SMS inside aligned ePCL scaffolds on the (A) x-z and (B) y-z planes. HE staining of seeded SMS inside aligned ePCL scaffolds on the (C) x-z and (D) y-z planes. (E) Coherency analysis and (F) the distribution (x-z plane as representative) of GFP alignment of seeded SMS inside two-layer aligned ePCL scaffolds (n=3). *$p < 0.01$. Error bar = SD. Scale bar = 100 μm. SM = Skeletal Muscle. Not e: Fig. 5 and Fig. 7 are the same locations. ⊗ = alignment perpendicular to the cross section. ↔ = alignment parallel to the cross section.

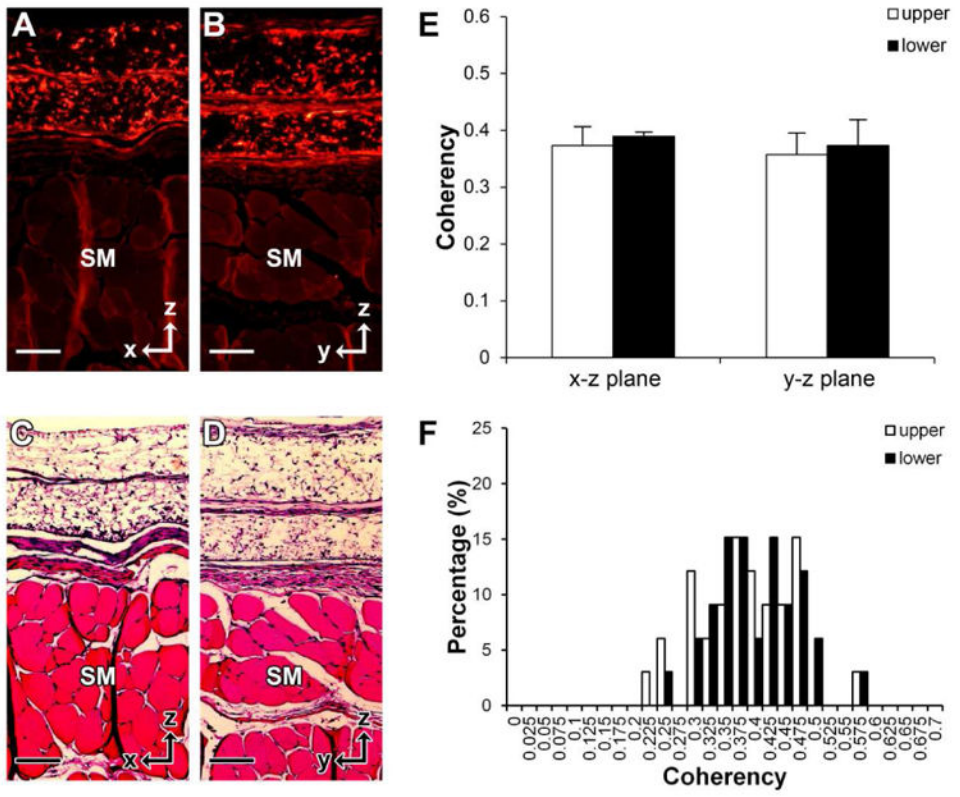

Fig. 8.

Quantification of GFP alignment of seeded SMS inside two-layer ePCL scaffolds with randomly oriented fibers. ePCL scaffolds were cultured *in vitro* for 3 weeks and retrieved on day 4 after implantation. GFP expression of seeded SMS inside randomly oriented ePCL scaffolds on the (A) x-z and (B) y-z planes. HE staining of seeded SMS inside randomly oriented ePCL scaffolds on the (C) x-z and (D) y-z planes. (E) Coherency analysis and (F) the distribution (x-z plane as representative) of GFP alignment of seeded SMS inside two-layer random ePCL scaffolds (n=3). $p > 0.01$. Error bar = SD. Scale bar = 100 μm. SM = Skeletal Muscle. Note: Fig. 6 and Fig. 8 are the same locations.